Journal of Analytical and Applied Pyrolysis 177 (2024) 106330

Contents lists available at ScienceDirect

Journal of Analytical and Applied Pyrolysis

journal homepage: www.elsevier.com/locate/jaap

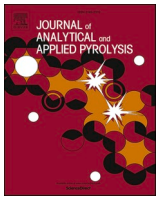

Synthesis of value-added aromatic chemicals from catalytic pyrolysis of waste wind turbine blades and their kinetic analysis using artificial neural network

Samy Yousef [a,*], Justas Eimontas [b], Nerijus Striūgas [b], Mohammed Ali Abdelnaby [c]

[a] Department of Production Engineering, Faculty of Mechanical Engineering and Design, Kaunas University of Technology, LT-51424 Kaunas, Lithuania
[b] Lithuanian Energy Institute, Laboratory of Combustion Processes, Breslaujos 3, LT-44403 Kaunas, Lithuania
[c] Mechatronics Systems Engineering Department, October University for Modern Sciences and Arts-MSA, Giza, Egypt

ARTICLE INFO

Keywords:
Waste wind turbine blades
Catalytic pyrolysis
Value-added aromatic chemicals
Artificial neural network
Catalytic pyrolysis kinetics

ABSTRACT

This research aims to convert the resin fraction of waste wind turbine blades (WTB) into value-added aromatic chemicals using catalytic pyrolysis. The catalytic study on WTB made of glass fibre/unsaturated polyester resin (UPR) was performed on two different types of zeolite catalysts (ZSM-5 and Y-type) using a thermogravimetric (TG) analyser. The effect of catalyst and heating rate on the abundance and composition of the synthesised aromatic chemicals was observed using TG-FTIR and GC/MS. The kinetics and thermodynamic behaviour of catalytic pyrolysis of WTB was also studied using traditional modelling techniques (KAS, FWO, Friedman, Vyazovkin, and Cai) and an artificial neural network (ANN). TG-FTIR results showed that the gases released from the catalytic process were very rich in aromatic groups, while GC/MS analysis revealed that benzene, toluene, and ethylbenzene (BTE) were the main constituents of the synthesised aromatic chemicals with abundance estimated at 36% (ZSM-5 at 10°C/min) and 64% (Y-type at 15°C/min) accompanied by a significant reduction in styrene formation up to 16.2% (main toxic element in the UPR). Besides, it contributed to reduction of the activation energy of the reaction up to 126 KJ/mol (ZSM-5) and 100 KJ/mol (Y-type). The trained ANN model also showed high performance in predicting the thermal decomposition zones of WTB at unknown heating rates with R^2 close to 1. Accordingly, the use of catalytic pyrolysis of WTB over a Y-type zeolite catalyst is highly recommended for decomposition of UPR to aromatic chemicals BTE and reduction of styrene in the produced fuel.

1. Introduction

Recently, waste wind turbine blades (WTB) have become a global challenge due to their huge quantity estimated at millions of tons [1] and their complex fibre-reinforced polymers structure, what makes landfill the most common method of disposal [2]. However, these practices waste many opportunities and resources that need to be preserved for future generations [3,4]. Therefore, their environmental and economic disadvantages served as a strong motivation for researchers to devise some solutions that could contribute to achievement of some benefits [5,6]. Pyrolysis is one of such solutions that has been widely investigated in the literature in various research directions, where the thermochemical experiments were conducted on WTB with different composition and scales. Since WTB are known as fibre reinforced polymer composites (FRPs), the first research direction is focused on studying the fundamental pyrolysis behaviour (using thermogravimetric analyser) of FRPs and neat FRPs samples were manufactured in the laboratory to serve as basic guidelines for comparison with commercial FRPs composites [7,8]. Also, the effect of additives (such as carbon black, graphene, carbon nanotubes, etc.) was taken into account in this direction [9,10]. In addition, the catalytic pyrolysis of the neat FRP samples over several types of zeolite catalysts were investigated [11–13]. The fundamental results showed that resin can decompose into its original chemical compound (phenol) and additives, while catalysts can contribute strongly to enhancement of number of phenols and aromatic compounds based on Gas chromatography-mass spectrometry (GC/MS).

Based on the promising fundamental results of pyrolysis of neat

* Corresponding author.
E-mail address: ahmed.saed@ktu.lt (S. Yousef).

https://doi.org/10.1016/j.jaap.2023.106330
Received 8 November 2023; Received in revised form 14 December 2023; Accepted 25 December 2023
Available online 28 December 2023

FRPs, the studies of pyrolysis of commercial FRPs in general and those used in production of wind turbine blades in particular were started [14,15], thus, making it possible to identify the effect of hygrothermal aging and coating gelcoat layer of WTB on their pyrolysis properties, kinetics, and distribution of chemical compounds resulting from their decomposition [16–18]. The studies in this category were focused on WTB of various compositions consisting mainly of epoxy resin/carbon fibre and epoxy resin/glass fibre. The results showed that the type of used fibre does not affect decomposition results because of its high thermal resistance, while resin is the key player in decomposition process [19,20]. Epoxy and polyester resin are among the most commercially thermosetting resins used in manufacture of wind blades [21]. The fast-heating pyrolysis characteristics of WTB contains epoxy resin was studied using a lab-scale fixed-bed reactor. The obtained oil product was rich in Bisphenol A with high selectivity (upto 50%), that can be reused for epoxy resins production again [22]. Also, the influences of core components of WTB based on epoxy resin on the evolution of pyrolysis products were studied [23]. The pyrolysis mechanisms of epoxy resin was simulated using ReaxFF-MD approach [24]. However, polyester resin is inexpensive with good toughening and fatigue performance, making it a strategic choice for blade manufacturers [25,26]. Polyester resins are rich in styrene and can be found in the form of saturated polyester resin (SPR) or unsaturated polyester resin (UPR) [27]. The SPR lack unsaturated double bonds and crosslink through ester linkages. In contrast, the UPR contain unsaturated double bonds and crosslink through free-radical polymerisation with higher chemical stability compared to the SPR type making it the first choice in the production of composite materials [28,29]. Also, this high demand for UPR has made studies focus more on UPR pyrolysis, while SPR pyrolysis has been ignored in the literature. Styrene is also the main component in UPR and thermogravimetry (TG) and GC/MS analysis showed that it can be recovered using a pyrolysis process at a lower temperature with less activation energy compared to epoxy resin [30]. Accordingly, the experiments were repeated again on a large scale with a 250 g reactor to determine the extent of destruction of final products and their gaseous compositions [31]. The study succeeded in converting UPR into oil rich in styrene by up to 49% at 500 °C without producing gaseous products. However, styrene is a highly toxic and polluting element, and its presence in oil can cause a lot of emissions and environmental pollution when burned [32,33].

Therefore, the option to dismantle styrene into its primary elements or aromatic components contributes effectively for alleviation of these effects and increase in its calorific value [34]. Within this context, the process of catalytic pyrolysis was used for this purpose and to convert styrene into aromatic substances [35]. Unfortunately, there are no studies in the literature on catalytic pyrolysis of UPR and its composite structure. However, the catalytic pyrolysis of different types of resins, such as epoxy resin composites over ZSM-5, HZSM-5, and HY zeolite catalyst, was studied [11,36]. The results revealed that ZSM-5 catalyst has high performance in terms of high recovery rate of phenol and aromatic chemicals in general, especially at catalyst-to-feedstock ratio (w/w) = 2. In addition, there are some studies that have employed catalytic pyrolysis HZSM-5 zeolite catalyst to recover styrene from some wastes rich in styrene, e.g., polystyrene waste and expanded polystyrene waste, followed by their decomposition into aromatic chemicals [37,38]. Also, the catalytic co-pyrolysis of biomass and polystyrene was studied together with metal-modified (Ga, Cobalt, Copper, Iron, Nickel) ZSM-5 zeolite catalysis to increase the abundance of aromatic compounds [35]. Since UPR is considered plastic waste, Y-zeolite was used a lot in this regard [39], however, this type of zeolite catalyst has not been explored yet in case of UPR. In order to explore the effect of adding of catalysts to thermal decomposition of fibres/UPR, this research aims to study the catalytic pyrolysis of WTB (fibres/UPR structure) over zeolite catalysts to decompose UPR into value-added aromatic chemicals. The catalytic conversion was performed with two different types of catalysts (ZSM-5 as a catalyst widely used to treat FRPs and Y-type as a common catalyst used to treat plastic waste) with WTB-to-catalyst ratio = 1:2. Also, the effect of these catalysts on number of synthesised aromatic chemicals, including benzene, toluene, and ethylbenzene (BTE), was observed using GC/MS. Meanwhile, the kinetic and thermodynamic characteristics of the catalytic pyrolysis process of WTB were investigated using various traditional modelling approaches (e.g., KAS, FWO, Friedman, Vyazovkin, and Cai) and advanced modelling approaches, particularly an artificial neural network (ANN), which can be used to train the recorded TG data and develop an ANN model to predict the thermal behaviour of WTB under unknown heating conditions [40]. Finally, the TG recorded data of catalytic pyrolysis of WTB were simulated using the Distributed activation energy (DAE) and independent parallel reactions (IPR) methods [41].

2. Experimental and methodology

2.1. Feedstock and catalysts

The WTB used in the present research with glass fibre/unsaturated polyester resin (GF/UPR) structure were acquired from the European Energy company, Denmark. The WTB were shredded to obtain small pieces, then grounded and sieved to obtain WTB powder with particles smaller than 500 μm. The WTB powder was dried under sunlight for 73 h to evaporate the moisture content and to get ready for the catalytic pyrolysis experiments using TGA. The UPR fraction of the prepared powder is rich in carbon (61 wt%) and volatiles matter (87 wt%), as shown in our previous study [30]. Meanwhile, ZSM-5 and Y-type zeolite catalysts were provided by Sigma-12 Aldrich Corp and all their properties are explained here [41,42]. The feedstocks were prepared by blending WTB with zeolite catalysts at a mixing ratio of raw material to catalyst = 1:2 based on the optimal results received from the literature [11,35]. Afterwards, the feedstocks could be prepared for future thermal experiments, as described in the following sections.

2.2. Thermogravimetric analysis

The TG analysis of the WTB over zeolite catalysts was carried out using TG: STA449 F3; NETZSCH, Selb, Germany on around 10 mg from each batch followed by determination of the weight loss-temperature profile of each sample in the range of room temperature to 900 °C during the catalytic pyrolysis. The TG analysis was conducted in pure nitrogen atmosphere with 60 mL/min flow rate to prevent oxidation of samples and to develop secondary reactions [43]. Also, the experiments were conducted using three different slow heating rates: in particular 5, 10, and 15 °C/min to study the effect of heating rate on the thermochemical behaviour of the samples, yield of the synthesised aromatic chemicals, and to evaluate the kinetics thermodynamic characteristics of the process [44]. Finally, Proteus software was employed to generate derivative thermogravimetry (DTG) data for each batch based on the TG measurements. Reproducibility of the measurements was ensured in every heating conditions to improve the accuracy of the results.

2.3. Catalytic pyrolysis performance index

The efficiency of catalytic pyrolysis of WTB was evaluated using the pyrolysis index (CPI) formula described in Eq. (1). In this formula, Rmax and Ravg are referring to maximum pyrolysis rate and average weight loss rate, respectively, while Tint, Tpeak, $\Delta T_{1/2}$, M_f are defined as initial devolatilization temperature, peak decomposition temperature, half-peak width temperature range (at R/R_{peak}= 0.5), and the residual mass of the decomposition process [45].

$$CPI = \frac{(-R_{max}) \times (-R_{avg}) \times M_f}{T_{int} \times T_{peak} \times \Delta T_{1/2}} \quad (1)$$

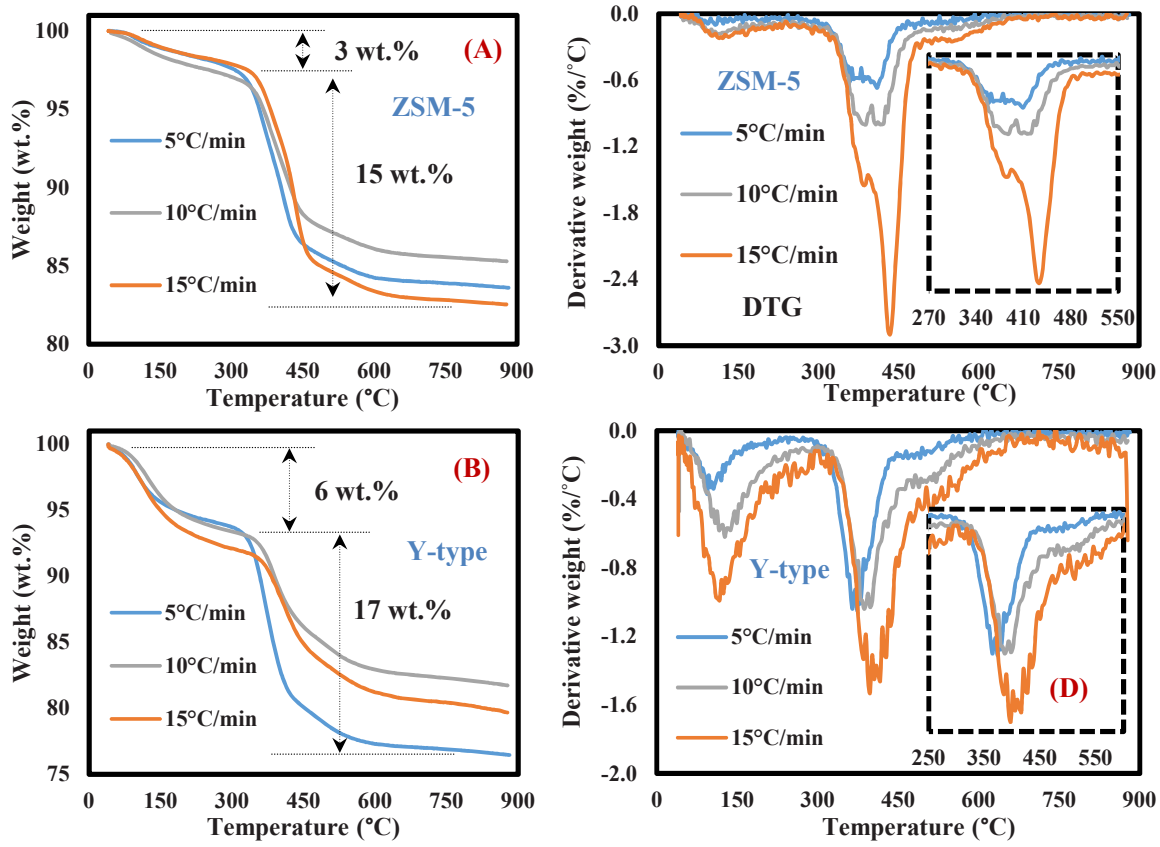

Fig. 1. (A, B) TGA curves and (C, D) DTG curves of WTB over zeolite catalysts.

Table 1
Catalytic pyrolysis characteristics of WTB samples over zeolite catalysts.

Parameter	5 °C/min	10 °C/min	15 °C/min	5 °C/min	10 °C/min	15 °C/min
	ZSM-5 zeolite sample			Y-type zeolite sample		
T_{int} (°C)	304	320	321	310	322	338
T_{peak} (°C)	409	421	433	373	397	397
R_{max} (%/min)	0.67	0.99	2.9	1.05	1.03	1.46
R_{avg} (%/min)	0.096	0.170	0.303	0.138	0.214	0.36
M_f (%)	82.54	85.29	83.6	79.69	81.74	76.47
$\Delta T_{1/2}$	90	93	61	63	67	80
CPI (%^{3} °C^{-3} min^{-2})	4.74E-07	1.15E-06	8.66E-06	1.59E-06	2.10E-06	3.74E-06

2.4. Chemical analysis of the synthesised aromatic chemicals

The functional groups of synthesised aromatic chemicals in vapour released from catalytic pyrolysis of WTB over zeolite catalysts were examined using FTIR coupled with TG device. Meanwhile, their chemical compounds, including benzene, toluene, ethylbenzene, etc. were identified and quantified using GC/MS (Shimadzu GC-2010, Kyoto, Japan). The measurements were carried out based on the conditions reported in the literature, briefly in the range of 30–600 m/s and column settings were argon gas, pressure = 20 psi, temperature = 95 °C, and time = 110 s [46].

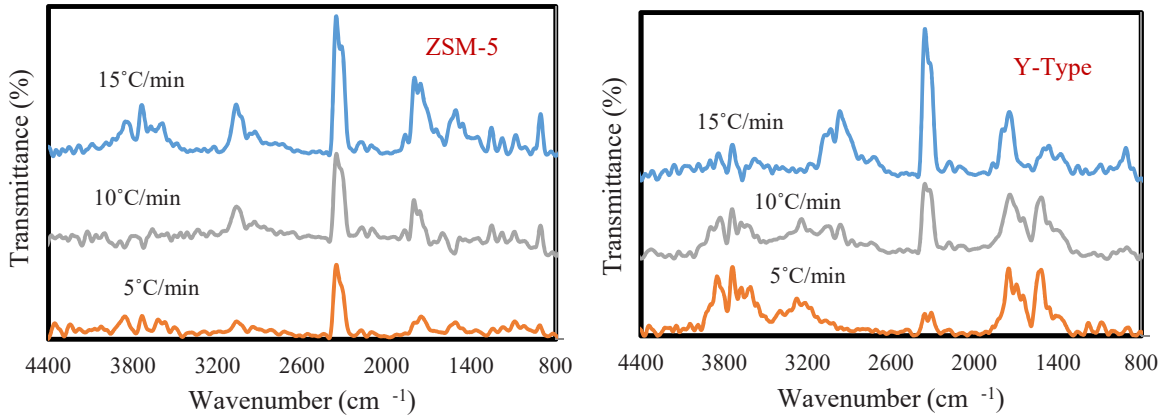

Fig. 2. 2D FTIR spectra of the aromatic chemicals generated from A) ZSM-5/WTB and B) Y-type/WTB samples.

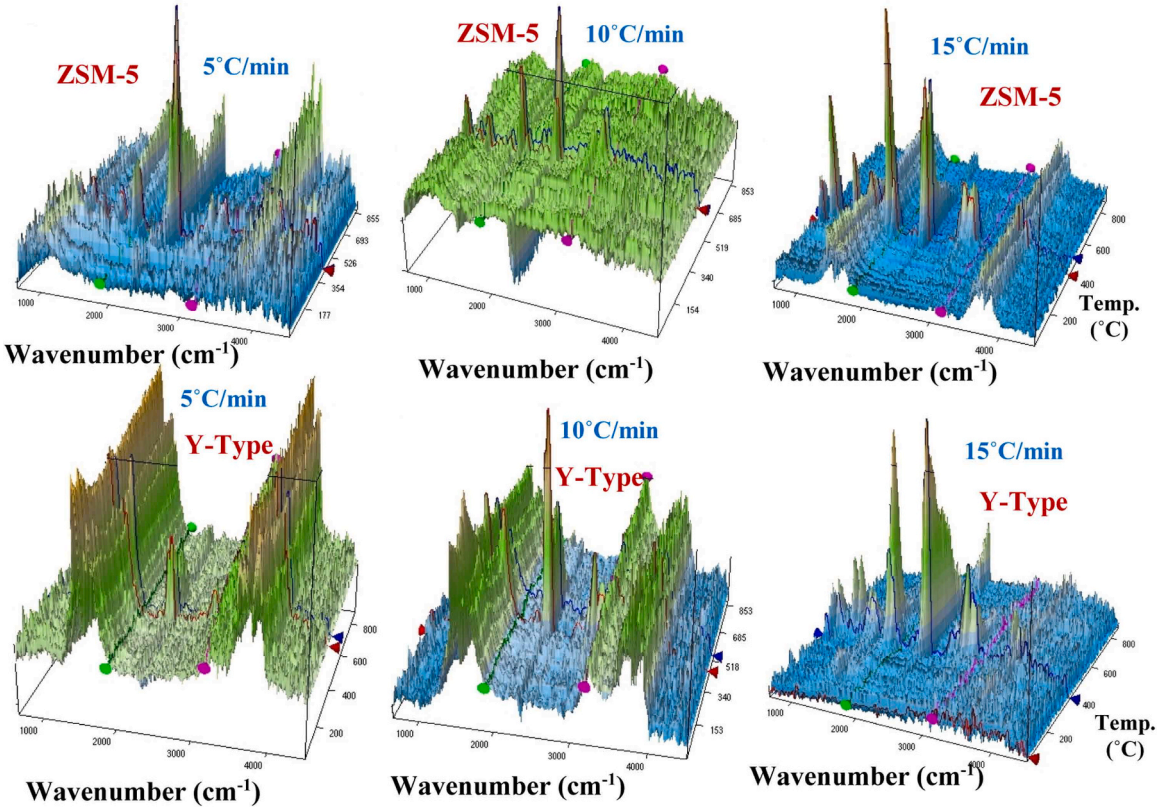

Fig. 3. 3D FTIR spectra of the aromatic chemicals generated from catalytic pyrolysis of WBT samples.

2.5. Mathematical model development for thermogravimetric analyses

2.5.1. Kinetic analysis

As mentioned above, the thermal decomposition process of WTB feedstock consisting of different components involves complex kinetics resulting from simultaneous production of numerous reaction stages. To understand the catalytic pyrolysis kinetics of WTB, several conventional and advanced mathematical approaches were applied. They can be used to evaluate their thermal behaviour and complexity. The formulas of conventional linear approaches (Model-free methods), including Kissinger-Akahira-Sunose (KAS), Flynn-Wall-Ozawa (FWO), and Friedman can be expressed using Eqs. (1)–(3) [47], respectively, while non-linear advanced optimisation approaches, including Vyazovkin and Cai methods, can be described using Eqs. (4) and (5)] [48], respectively. These models can be used to calculate activation energy (Ea) and pre-exponential factor (A) as a function of a conversion rate (α) based on a generic algorithm of a curve fitting and optimisation process.

$$\ln\left(\frac{\beta}{T^2}\right) = \ln\left(\frac{AR}{Eag(y)}\right) - \frac{-Ea}{RT} \quad , \tag{1}$$

$$\ln\beta = \left(\frac{\ln AEa}{Rgy}\right) - 5.335 - \frac{1.0516Ea}{RT} \tag{2}$$

$$\ln\left(\frac{\beta dy}{dT}\right) = \ln(Af(y))\left(\frac{-Ea}{RT}\right), \tag{3}$$

$$(\alpha) = \int_0^{\alpha} \frac{dy}{f(y)} = A\int_0^{t} \exp(-E/RT)dt \tag{4}$$

$$\ln\left\{\frac{\beta_i}{T_{y,i}^2\left[h(x_{y,i}) - \frac{x_{y,i}^2 e^{x_{y,i}}}{x_{y-\Delta y,i}^2 e^{x_{y-\Delta y,i}}} h(x_{y-\Delta y,i})\right]}\right\} = \ln\left\{\frac{A_{y-\Delta y/2}R}{E_{y-\Delta y/2}\ g(y, y-\Delta y)}\right\} - \frac{E_{y-\Delta y/2}}{RT_{y,i}} \tag{5}$$

2.5.2. Fitting of thermogravimetric profiles

The TG profiles of decomposed WTB feedstock over zeolite catalysts were simulated mathematically using the Distributed activation energy method (DAEM) and Eq. (6). The independent parallel reactions (IPR) were employed to simulate their DTG profiles at the specified heating conditions using Eq. (7), then checking their deviations (Dev.%) using Eq. (8) [49–51].

$$\ln\left(\frac{\beta}{T^2}\right) = \ln\left(\frac{AR}{Ea}\right) + 0.6075 - \frac{Ea}{RT}, \tag{6}$$

$$\frac{dm^{calc}}{dt} = -(m_0 - m)\sum_{i=1}^{3} .C_i\frac{dX_i}{dt} \tag{7}$$

$$\text{Dev.}(\%) = \frac{100\sqrt{\text{F.O.}_{DTG}(Z-N)}}{\max(|dm/dt|)} \tag{8}$$

2.5.3. Thermodynamic analysis

The thermodynamic behaviour the of the decomposed WTB feedstock over zeolite catalysts was studied to determine their thermodynamic characteristics, in particular enthalpy change (ΔH), Gibbs free energy change (ΔG), and entropy change (ΔS). These parameters were calculated with the help of Eqs. (9)–(12) [52]. In these formulas, K_B (1.3819×10^{-23} J/K), Tm, h (6.6269×1034 J s), and A refer to Boltzmann constant, maximum decomposition temperature (received

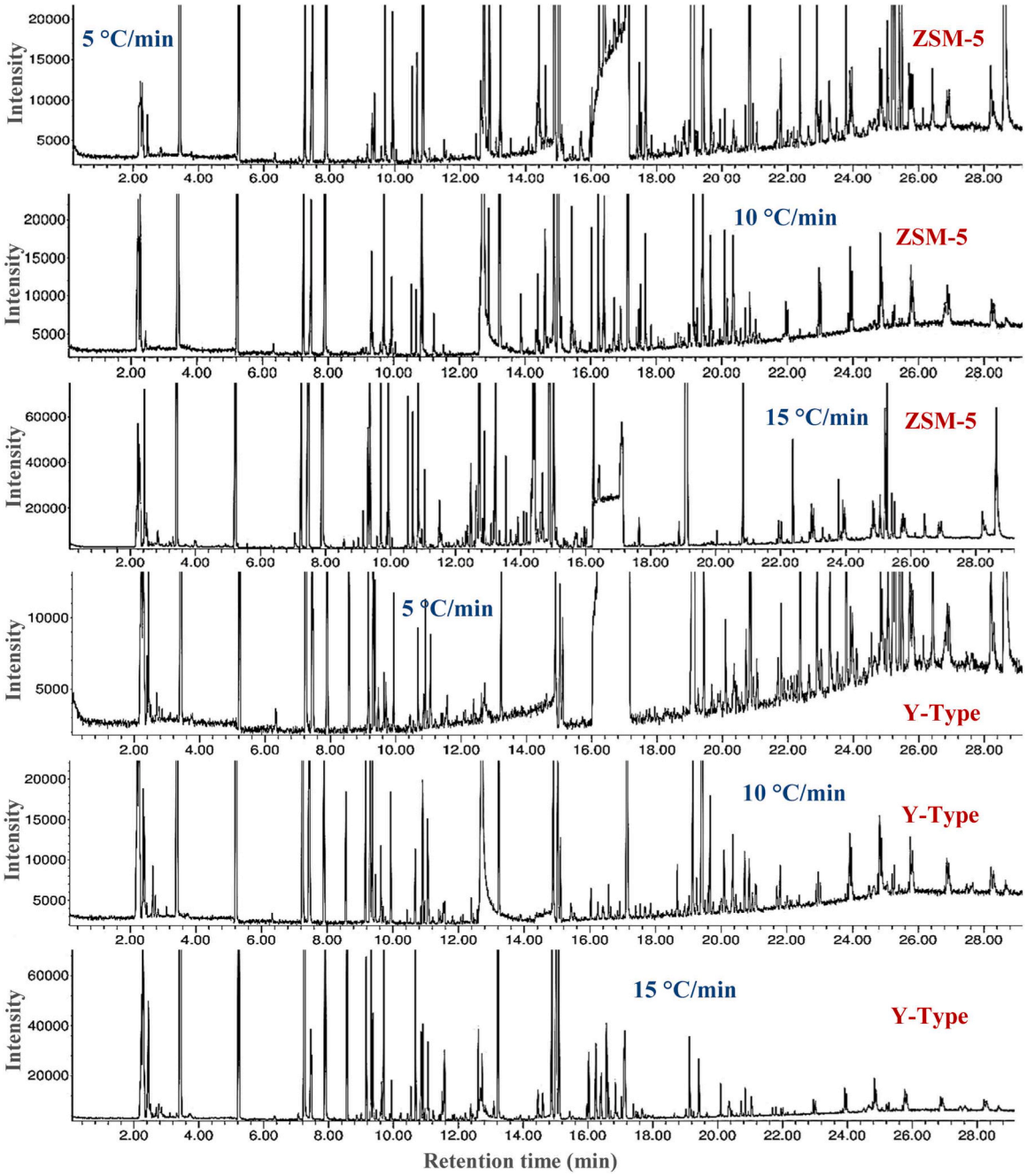

Fig. 4. GC/MS analysis of the generated vapours of WBT over zeolite catalysts.

from DTG curves), Planck's constant, and pre-exponential factor that can be extracted from kinetic analysis, respectively [53].

$$\Delta H = Ea - RT_m, \tag{9}$$

$$\Delta G = \mathrm{Ea} + RT_m \ln\left(\frac{K_B T_m}{hA}\right) \quad , \tag{10}$$

$$\Delta S = \frac{\Delta H - \Delta G}{T_m} \tag{11}$$

2.5.4. Development of artificial neural network

In this section, an artificial neural network (ANN) model was built using MATLAB® software to predict the weight loss of WTB feedstock over zeolite catalysts and to provide predictions for their nonlinear degradation profiles at other heating conditions. The ANN model was developed based on the feed-forward backpropagation method by defining three main layers: input, hidden, and output layers. The temperature (°C), heating rate (min/°C), and degree of conversion (α) were defined as the main parameters of input neuron, while weight loss (%) was considered as an output neuron of the model. Meanwhile, because of its high accuracy, the Levenberg–Marquardt back propagation algorithm was used to train the developed ANN model [39]. The model was built based on the following configuration: 70% for training, 15% for testing, and 15% for validation. Also, the input and output parameters were normalised before training process to improve the efficiency of the developed network. The trial-and-error technique was used to obtain the optimum neural network architecture [54]. The number of neurons in the hidden layer was calculated and optimised using the mean square error (MSE) method until ANN converged to a minimum error. The developed model was extended to predict thermal characteristics of

Table 2
GC/MS compounds generated from pyrolysis of WTB over ZSM-5 catalyst.

5°C/min			10°C/min			15°C/min		
Time (min)	GC Compounds	Area (%)	Time (min)	GC Compounds	Area (%)	Time (min)	GC Compounds	Area (%)
2.203	Borane carbonyl	0.61	2.203	Carbon dioxide	1.32	2.216	Propene	1.02
3.426	Benzene	7.57	2.274	Acetaldehyde	0.82	2.287	2-Butene, (Z)-	1.08
5.224	Toluene	3.96	3.419	Benzene	28.38	2.436	Propanal	1.13
7.255	Ethylbenzene	1.99	5.224	Toluene	5.36	3.419	Benzene	5.89
7.468	p-Xylene	1.35	7.255	Ethylbenzene	2.57	5.224	Toluene	5.58
7.895	Styrene	6.90	7.468	p-Xylene	1.00	7.248	Ethylbenzene	3.02
9.694	.alpha.-Methylstyrene	1.80	7.895	Styrene	9.40	7.468	p-Xylene	5.05
9.933	Benzene, 1,3,5-trimethyl-	0.61	9.700	.alpha.-Methylstyrene	1.32	7.895	Styrene	16.20
10.845	Indene	3.69	10.852	Indene	5.60	9.364	Benzene, 1-ethyl-2-methyl-	1.93
12.727	2-Methylindene	6.82	12.727	Benzene, (1-methyl-2-cyclopropen-1-yl)-	8.93	9.694	.alpha.-Methylstyrene	3.04
12.889	1,4-Dihydronaphthalene	0.89	13.226	Naphthalene	5.49	9.933	Benzene, 1,2,3-trimethyl-	1.06
13.225	Azulene	2.56	14.881	Naphthalene, 2-methyl-	7.52	10.535	Benzene, cyclopropyl-	0.98
14.390	2-Ethyl-1-H-indene	0.65	15.017	Phthalic anhydride	9.50	10.677	Indane	0.90
14.881	Naphthalene, 2-methyl-	5.48	15.431	Ethanone, 1-(4-ethylphenyl)-	0.89	10.845	Indene	4.81
15.011	Phthalic anhydride	10.60	16.240	Naphthalene, 1-ethyl-	1.59	12.727	Benzene, (1-methyl-2-cyclopropen-1-yl)-	6.56
16.240	Naphthalene, 2-ethyl-	2.12	16.408	Naphthalene, 1,5-dimethyl-	1.24	13.226	Azulene	1.87
16.402	Naphthalene, 2,7-dimethyl-	1.19	17.139	Cycloheptasiloxane, tetradecamethyl-	2.10	14.390	2-Ethyl-1-H-indene	4.89
17.107	Cycloheptasiloxane, tetradecamethyl-	4.46	17.669	Naphthalene, 2,3,6-trimethyl-	0.79	14.881	Naphthalene, 2-methyl-	7.71
17.669	Naphthalene, 1,4,6-trimethyl-	1.05	19.138	Silane, [[4-[1,2-bis[(trimethylsilyl) oxy]ethyl]− 1,2-phenylene]bis(oxy)] bis[trimethyl-	0.78	15.017	Phthalic anhydride	10.01
19.093	Cyclooctasiloxane, hexadecamethyl-	12.62	19.422	Benzene, 1,1′-(1,3-propanediyl)bis	4.47	16.240	Naphthalene, 1-ethyl-	1.13
19.422	Benzene, 1,1′-(1,3-propanediyl)bis	5.01	20.354	1,2-Diphenylcyclopropane	0.93	17.107	Cycloheptasiloxane, tetradecamethyl-	2.24
20.846	Cyclononasiloxane, octadecamethyl-	3.58				19.093	Cyclooctasiloxane, hexadecamethyl-	7.45
22.379	Cyclononasiloxane, octadecamethyl-	1.20				20.846	Cyclononasiloxane, octadecamethyl-	2.09
22.890	Naphthalene, 2-phenyl-	0.74				25.205	Anthracene, 9,10-dihydro-9-methyl-	0.90
23.782	Isoproterenol tri-TMS derivative	0.72				25.270	9 H-Fluorene, 9,9-dimethyl-	1.25
25.057	Sarcosine, N-isobutyryl-, tetradec yl ester	0.66				28.640	Triphenylphosphine oxide	2.21
25.205	Anthracene, 9,10-dihydro-9-methyl-	2.12						
25.270	Anthracene, 9,10-dihydro-9-(.alpha.-methylbenzyl)-	3.02						
25.406	Anthracene, 9,10-dihydro-	0.87						
25.496	4-([(Furan-2-ylmethyl)-amino]-methyl)− 3,5-dimethyl-1 H-pyrrole-2-carboxylic acid ethyl ester	0.72						
28.640	Triphenylphosphine oxide	4.44						

WTB at heating rates (7 °C/min and 12 °C/min) that were not measured experimentally during TG experiments. These unknown heating rates were set in the ranges specified at the beginning of the research (5–15 °C/min).

3. Results and discussion

3.1. Thermogravimetric analysis and characteristics

Fig. 1A and B shows thermal decomposition of WTB feedstock over ZSM-5 and Y-type zeolite catalysts, respectively, with varying heating rates. As shown, both samples provide a high thermal stability up to 100 °C followed by a small drop up to 160 °C (< 3 wt%) as a result of evaporation of moisture content in WTB feed materials and used catalysts. Afterwards, the samples started to decompose at several temperatures in three different boundaries: in particular, at 350 °C (< 7 wt%), as a result of evaporation of remaining chemicals during different fabrication processes; at 460 °C (< 12 wt%) as a result of degradation of UPR and a coat layer's sub-components; and at 600 °C (< 3 wt%) due to ash formulation. Compared to thermal decomposition of WTB (550 °C) without catalyst [30], the catalytic pyrolysis of WTB showed a higher degradation temperature up to 600 °C. Also, it was noticed that both samples have almost similar degeneration features with total weight loss of 18 wt% (ZSM-5) and 23 wt% (Y-type). This weight loss is attributed to decomposition of resin and a coating layer only, because in the last stage of the reaction (devolatilization), fibres remained in the form of solid residues [9,10]. Although the Y-type catalyst provides higher weight loss, this value can be a little deceptive since UPR in the samples may be slightly higher than that in case of the ZSM-5 catalyst. However, this deceptive result does not affect the subsequent kinetic calculations and calculated activation energy, which refers to the energy required to decompose the organic components (UPR) in the feedstock only [29,30], while the solid residues including fibres and ZSM-5 catalyst cannot decompose at this low decomposition temperature [11,55]. It was observed that the amount of solid residues was very high because this residual fraction included the weight of the catalyst with a high melting temperature [11,56]. Meanwhile, the thermograms with individual DTG at specific heating rates showed only a single peak in the ranges of 409–433 °C in case of ZSM-5 catalyst samples (Fig. 1C). The same features were observed in case of Y-type (Fig. 1D), but the peak temperature decreased significantly up to 397 °C. Also, due to its hydrated and unique porous structure containing water molecules, the Y-type sample

Table 3
GC/MS compounds generated from pyrolysis of WTB over Y-type catalyst.

5°C/min			10°C/min			15°C/min		
Time (min)	GC Compounds	Area (%)	Time (min)	GC Compounds	Area (%)	Time (min)	GC Compounds	Area (%)
2.209	Ethylene oxide	1.12	2.216	Propene	1.33	2.287	Propane	1.78
2.281	Propane	1.02	2.274	Isobutane	1.19	3.425	Benzene	16.07
2.436	Propanal	0.55	3.419	Benzene	20.57	5.224	Toluene	10.59
3.419	Benzene	9.57	5.224	Toluene	10.82	7.255	Ethylbenzene	37.34
5.224	Toluene	4.92	7.255	Ethylbenzene	28.81	7.895	Styrene	10.95
7.248	Ethylbenzene	18.58	7.455	p-Xylene	3.28	8.568	Benzene, (1-methylethyl)-	2.54
7.455	p-Xylene	1.29	7.908	Cyclopentene, 1-ethenyl-3-methylene-	2.03	9.163	Benzene, propyl-	1.21
7.902	Styrene	1.67	8.568	Benzene, (1-methylethyl)-	0.82	9.305	Benzene, 1-ethyl-3-methyl-	1.27
8.568	Benzene, (1-methylethyl)-	0.78	9.163	Benzene, propyl-	1.10	9.700	.alpha.-Methylstyrene	1.44
9.163	Benzene, propyl-	0.55	9.306	Benzene, 1-ethyl-2-methyl-	2.01	10.677	Indane	1.33
9.306	Benzene, 1-ethyl-2-methyl-	0.87	9.370	Benzene, 1-ethyl-3-methyl-	1.09	13.225	Azulene	3.85
13.226	Naphthalene	0.84	9.933	Benzene, 1,2,3-trimethyl-	0.80	14.881	Naphthalene, 2-methyl-	4.01
14.881	Naphthalene, 1-methyl-	1.07	10.903	Benzene, 1,2-diethyl-	0.80	15.011	Phthalic anhydride	4.32
15.017	Phthalic anhydride	0.58	11.065	Benzene, 2-ethyl-1,3-dimethyl-	0.83	15.108	Naphthalene, 1-methyl-	1.70
17.107	Cycloheptasiloxane, tetradecamethyl-	5.92	12.727	Benzoic acid	8.44	17.132	Cycloheptasiloxane, tetradecamethyl-	1.59
19.093	Cyclooctasiloxane, hexadecamethyl-	20.89	13.226	Naphthalene	1.39			
19.422	Benzene, 1,1′-(1,3-propanediyl)bis	1.12	14.881	Naphthalene, 1-methyl-	1.62			
20.846	Cyclononasiloxane, octadecamethyl-	5.98	15.024	Phthalic anhydride	1.30			
22.379	Cyclononasiloxane, octadecamethyl-	2.04	17.133	Cycloheptasiloxane, tetradecamethyl-	3.04			
22.890	Naphthalene, 2-phenyl-	1.10	19.131	Silane, [[4-[1,2-bis[(trimethylsilyl)oxy] ethyl]− 1,2-phenylene]bis(oxy)]bis [trimethyl-	1.11			
23.278	4,4′-(Hexafluoroisopropylidene) diphenol	0.62	19.416	Benzene, 1,1′-(1,3-propanediyl)bis	6.90			
23.782	Cyclononasiloxane, octadecamethyl-	1.28	20.354	1,2-Diphenylcyclopropane	0.73			
25.063	Sarcosine, N-isobutyryl-, tetradecyl ester	1.18						
25.205	Benzo[*f*]quinoline	2.78						
25.270	Benzo[*f*]quinoline	3.90						
25.412	Phenanthrene, 9,10-dihydro-	1.07						
25.497	cis-Stilbene	0.93						
26.428	Acetamide, 2-(adamantan-1-yl)-N-(1-adamantan-1-ylethyl)-	0.69						
28.207	Sarcosine, N-isobutyryl-, tetradecyl ester	0.67						
28.640	Triphenylphosphine oxide	6.40						

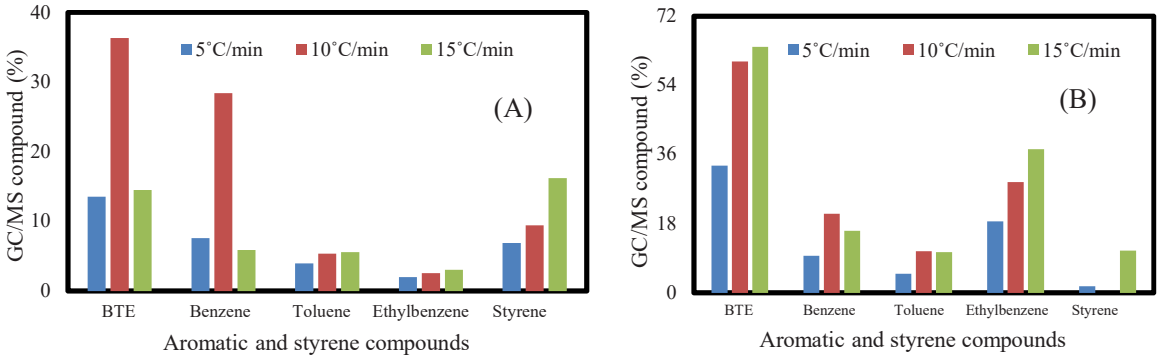

Fig. 5. Concentration of aromatic and styrene compounds in the vapours generated from A) ZSM-5 and B) Y-type zeolite samples.

showed another weak peak at 117 °C. The water content can be removed through evaporation during the decomposition process with the help of desorption and dehydroxylation reactions with high weight loss [57]. Also, it was observed that intensity of the maximum heating peaks of both samples depended on release of bigger heat flux that led to faster heat exchange in the resin molecules [58], and these results are consistent with the results of TGA. Finally, all catalytic pyrolysis characteristics of WTBs samples and their CPI values are summarised in Table 1. As shown in the calculations, the highest heating rate (15 °C/min) reflects higher CPI values estimated at 8.66 E-06%^{3} °C^{-3} min^{-2} (ZSM-5) and 3.74 E-06%^{3} °C^{-3} min^{-2} (Y-type), which means that performance of the catalytic pyrolysis process of WTB can be improved by raising the heating conditions while maximum and average decomposition rates increase significantly, as shown by the DTG results at this heating rate.

3.2. TG-FTIR and GC/MS analysis of the synthesised aromatic chemicals

Fig. 2 shows the 2D-FTIR spectra of aromatic chemicals generated from the catalytic pyrolysis of ZSM-5/WTB and Y-type/WTB samples

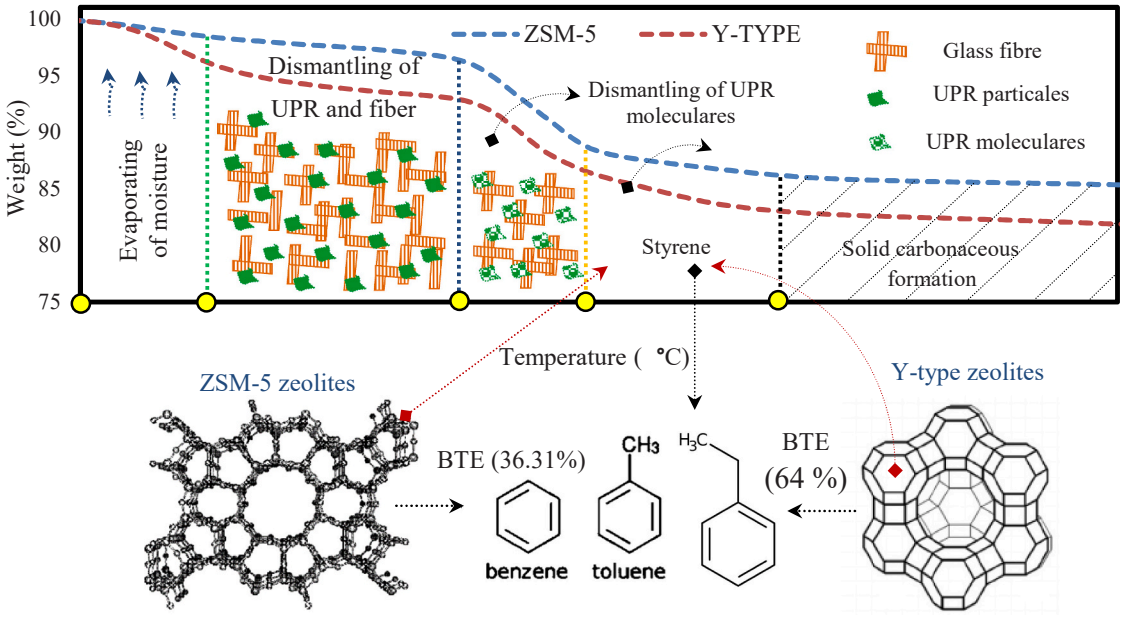

Fig. 6. Mechanism of WTBs catalytic pyrolysis over zeolite catalysts.

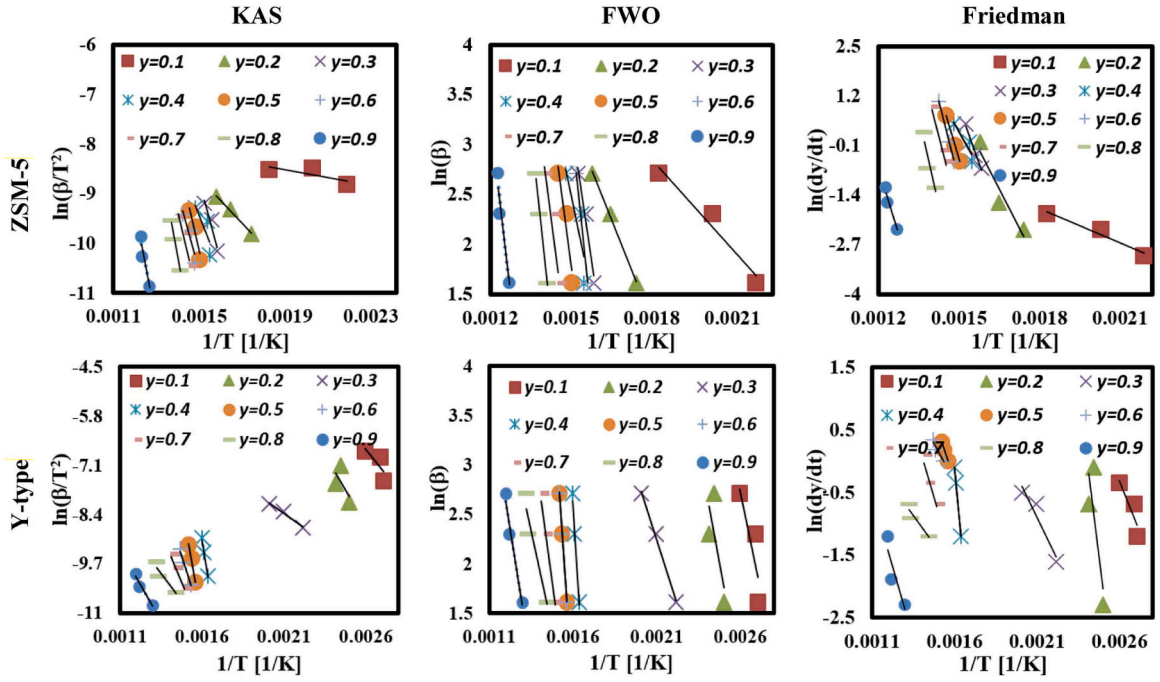

Fig. 7. Isoconversional plots (KAS, FWO, and Friedman) of ZSM-5/WTB and Y-type/WTB samples.

under the mentioned heating conditions (5, 10, 15 °C/min). The FTIR spectrum of sample ZSM-5/WTB (Fig. 2A) shows three major functional groups at 2350 cm^{-1} (CO_2), 3045 cm^{-1} (C-H stretch), and 1796 cm^{-1} (C═O stretching), in addition to some weak peaks at 3739 cm^{-1} (O-H stretching) and 800–1200 cm^{-1} (aromatic hydrocarbons). The presence of main functional groups indicates that the catalytic pyrolysis vapour is rich in aromatics, alkanes, ketones, aldehydes and carboxylic acid compounds [59]. Also, it was noticed that absorbances of these groups increased with raising heating rate due to enhanced heat flux and heat exchange. Meanwhile, the Y-type/WTB sample showed similar FTIR spectra (Fig. 2B) with the same functional groups but with slightly higher absorbances, especially in case of aromatic hydrocarbons. Whereas the 3D-FTIR spectra of the samples (Fig. 3) manifested changes in the peak absorbances as a function of decomposition temperature and heating rate. As the heating rate increases, the FTIR peaks become smoother and exhibit less noise, what indication that most of the sub-components (like coating layer and other additives) of the substance WTBs have decomposed into vapour. Where the higher heating rates tend to result in a more consistent and smoother response in the FTIR peaks, which indicates a more efficient or complete decomposition of the organic components into vapour [60,61].

Fig. 4 shows GC/MS spectra of synthesised aromatic chemicals in the generated vapour for catalytic pyrolysis of WTB over ZSM-5 and Y-type zeolite catalysts. The intensities of these GC compounds at different heating rates are shown in Tables 2 and 3. The GC/MS results unveiled that predominant compounds in generated vapour differ, in particular,

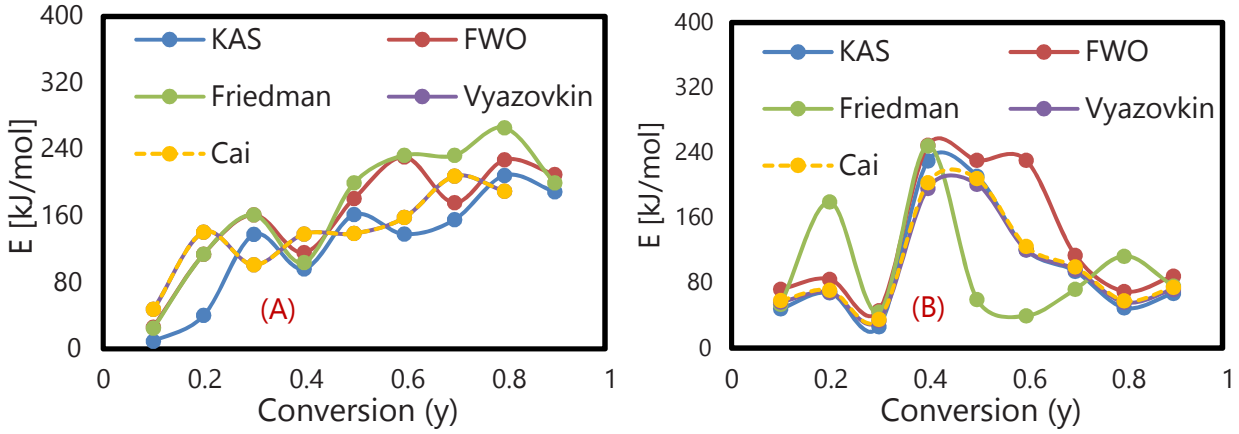

Fig. 8. The relationship between the computed Ea with conversion of A) ZSM-5/WTB and B) Y-type/WTB sample.

Table 4
The computed activation energy of ZSM-5/WTB and Y-type/WTB samples.

y	*KAS*			*FWO*			*Friedman*			*Vyazovkin*		*Cai*	
	Ea (KJ/mol)	R^2	*A* (1/s)	*Ea* (KJ/mol)	R^2	*A* (1/s)	*Ea* (KJ/mol)	R^2	*A* (1/s)	*Ea* (KJ/mol)	R^2	*Ea* (KJ/mol)	R^2
ZSM-5/WTB sample													
0.1	9.03	0.66	1.10E + 05	26.23	0.95	2.98E + 05	24.94	0.96	2.01E + 03	15.90	0.89	15.90	0.90
0.2	40.22	0.99	1.37E + 02	113.90	1.00	1.11E + 07	113.90	0.90	3.30E + 10	47.52	1.00	47.52	1.00
0.3	137.53	0.94	1.34E + 07	161.29	0.96	1.36E + 40	161.29	0.97	1.19E + 14	140.43	0.96	140.43	0.95
0.4	96.09	0.69	6.85E + 03	115.76	0.74	3.02E + 10	103.76	0.84	1.12E + 09	100.98	0.70	100.98	0.70
0.5	161.38	0.88	9.66E + 07	180.98	0.90	3.16E + 14	199.54	1.00	1.72E + 16	138.17	0.92	138.17	0.90
0.6	138.02	0.81	1.23E + 06	230.82	1.00	4.83E + 18	232.79	1.00	4.83E + 18	138.79	0.87	138.79	0.83
0.7	155.36	0.91	6.67E + 06	175.73	0.93	9.88E + 01	232.79	0.95	1.77E + 17	157.97	0.97	157.97	0.92
0.8	208.71	0.98	1.52E + 10	227.32	0.99	4.98E + 16	266.05	0.82	2.72E + 18	207.85	1.00	207.85	0.99
0.9	188.98	0.91	1.10E + 07	209.83	0.93	9.75E + 13	199.54	0.93	1.79E + 12	189.56	0.93	189.56	0.92
Avg.	126.15	0.86	1.71E + 09	160.21	0.93	1.51E + 39	170.51	0.93	8.60E + 17	126.35	0.91	126.35	0.90
Y-type/WTB sample													
0.1	48.52	0.66	2.21E + 05	72.42	0.75	2.65E + 12	53.79	0.78	1.47E + 09	56.48	0.79	58.48	0.72
0.2	67.93	0.74	5.51E + 05	84.75	0.56	1.80E + 12	179.66	0.67	8.21E + 05	68.76	0.77	71.20	0.69
0.3	26.56	0.98	8.21E + 01	46.15	1.00	4.12E + 09	44.39	0.92	1.22E + 03	34.04	0.99	35.24	0.99
0.4	230.02	0.98	6.84E + 04	249.18	0.98	1.13E + 05	248.59	1.00	3.74E + 05	196.44	0.97	203.39	0.97
0.5	211.11	1.00	3.51E + 12	230.70	1.00	6.96E + 18	59.86	1.00	4.39E + 03	201.27	0.99	208.39	1.00
0.6	120.86	0.97	1.50E + 05	230.70	1.00	1.16E + 19	39.66	1.00	4.52E + 05	120.76	0.97	125.04	0.97
0.7	94.32	0.97	6.10E + 02	114.26	0.98	2.69E + 09	72.33	0.95	1.01E + 02	96.56	0.96	99.98	0.97
0.8	49.50	0.90	1.56E + 01	69.81	0.92	6.91E + 05	113.07	0.09	6.03E + 00	56.35	0.87	58.35	0.89
0.9	67.40	0.95	2.98E + 00	88.65	0.97	2.99E + 06	76.24	0.86	2.98E + 00	72.19	0.80	74.75	0.88
Avg.	101.80	0.90	3.90E + 11	131.85	0.91	2.07E + 18	98.62	0.81	1.64E + 08	100.32	0.90	103.87	0.90

these are benzene, toluene, and ethylbenzene (BTE). The abundance of BTE compounds was affected significantly by two main factors: catalyst type and heating rate. The highest abundance of BTE compounds was obtained using Y-type (64% at 15 °C/min) compared to 36.31% in case of ZSM-5 (at 10°C/min), as shown in Fig. 5. As shown, the most abundant benzene compound was obtained at 10 °C/min, where at the lowest heating rate, benzene tends to form with appropriate selectivity [62]. Meanwhile, the shape-selective ZSM-5 catalyst leads to the retention and rearrangement of benzene rings [63,64], which contributes to increased aromatic compound formation compared to 15 °C/min. Also, a small percentage of styrene compounds was observed in both cases, reaching 10.95% at 15 °C/min (Y-type) and 16.2% at 15 °C/min (ZSM-5). Meanwhile, the Y-type catalyst successfully eliminated styrene completely at 10 °C/min and decomposed it into BTE compounds that could be used in petrochemical, pharmaceutical and energy industries [65,66]. Accordingly, Y-type catalyst is highly recommended to decompose WTB at 15 °C/min into BTE-rich compounds with promising yields of more than 64%. Also, this catalyst showed higher performance in reducing styrene in catalytic pyrolysis vapour compared to the vapour and oil products obtained from WTB pyrolysis which provides a high amount of styrene compounds up to 62% [29,30].

3.3. Catalytic pyrolysis mechanism of WTBs

Catalytic pyrolysis of WTB is a complex process because it contains several organic components, including fibres, UPR and their contents, and a gelcoat coat layer bonded with the fibre as a solid fraction [30,67]. Under applied processing, these organic compounds decompose together in parallel or series reactions, making it difficult to understand the mechanism of their thermal decomposition. In order to circumvent this complexity, the catalytic pyrolysis mechanism of WTBs over ZSM-5 at 10 °C/min and Y-type zeolite catalysts at 15 °C/min (which provides higher BTE abundance in both samples) was studied based on the characteristics obtained from TGA experimental measurements and the suggested diagram of their mechanisms is shown in Fig. 6. The diagram showed that both samples and catalysts exhibited resistance to degeneration up to 100 °C followed by moisture evaporating up to 150 °C, however, Y-type zeolite seemed to have higher moisture content (due to its hydrated structure, as listed above), and thus, bigger drop in this zone [56]. In the next zone (150–350 °C), the UPR and coat layer started to dismantle from fibre fractions (undegradable short fibre) and broke down their chemical and mechanical bonds, then evaporating the chemical residues in them. The dismantled UPR and coat debris started

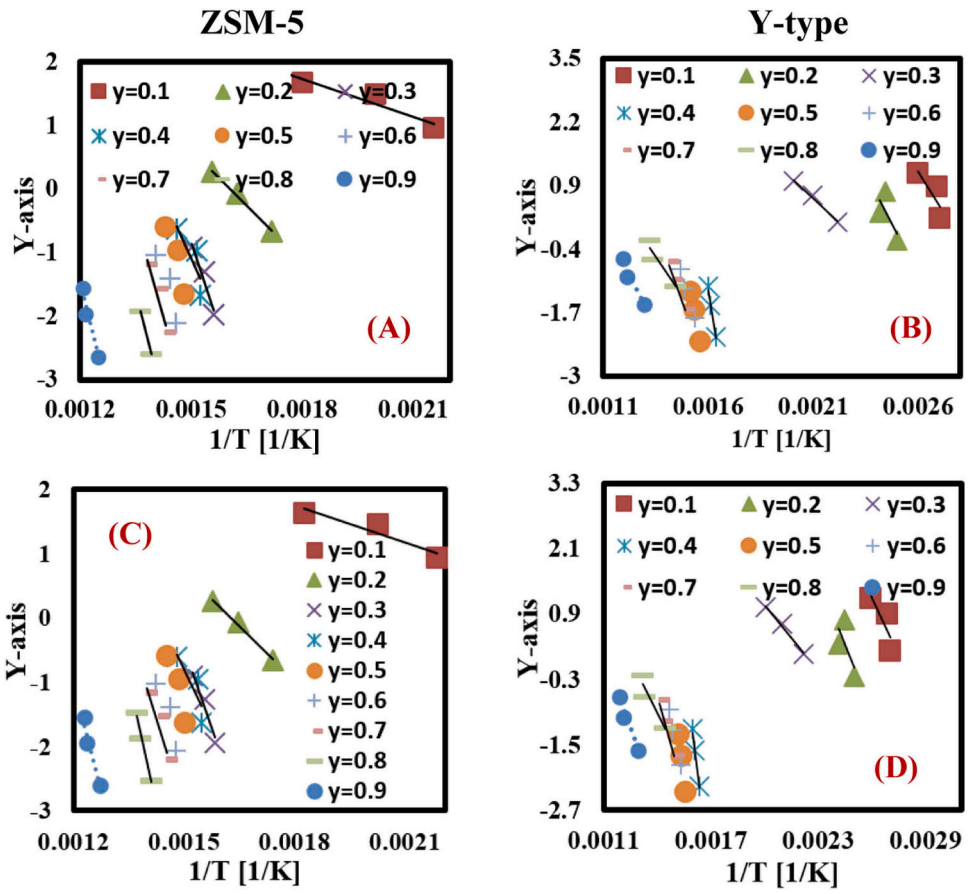

Fig. 9. (A, B) Vyazovkin and (C, D) Cai plots of curves of ZSM-5/WTB and Y-type/WTB samples.

Table 5
Thermodynamic parameters of WTB catalytic pyrolysis.

y	*KAS*						*FWO*						*Friedman*					
	ΔH (kJ/mol)		ΔG (kJ/mol)		ΔS (J/mol K)		ΔH (kJ/mol)		ΔG (kJ/mol)		ΔS (J/mol K)		ΔH (kJ/mol)		ΔG (kJ/mol)		ΔS (J/mol K)	
	ZSM	Y	ZSM	Y	ZSM	Y	ZSM	Y	ZSM	Y	ZSM	Y	ZSM	48	ZSM	Y	ZSM	Y
0.1	3	43	-99	-52	5	64	20	67	128	63	29	100	19	174	163	3	26	72
0.2	34	62	-106	-27	50	93	108	79	195	73	156	118	108	39	151	87	147	260
0.3	132	21	57	-117	190	32	156	41	-197	1	224	61	155	243	149	-85	212	58
0.4	90	224	-28	123	130	335	110	244	151	145	158	363	98	54	162	151	133	362
0.5	156	206	93	203	224	306	175	225	163	304	252	336	193	34	157	-62	264	81
0.6	132	115	44	19	190	172	225	225	157	307	324	336	227	67	156	-56	310	51
0.7	150	89	71	-39	215	133	170	109	324	67	244	162	227	107	176	-71	310	100
0.8	203	44	169	-104	292	66	222	64	180	-24	319	96	260	71	193	-46	355	161
0.9	183	62	108	-95	264	92	204	83	199	3	294	124	193	93	213	-86	264	106
Avg.	120	96	34	-10	173	144	204	126	145	104	222	188	164	48	169	-18	225	139

to dismantle again into smaller molecules up to 450 °C by overcoming their Van der Waals bonds [68]. In the next stage (up to 590 °C), UPR with smaller molecules and lower crystallinity decomposed completely into its original styrene compound [29]. The catalyst involved in the reaction led to dehydroxylation followed by cracking of styrene into its main BTE compounds [69]. As shown, Y-type zeolite catalyst provides larger abundance of aromatic hydrocarbons (BTE) compared to ZSM-5 catalyst due to its larger porosity and acidity that allowed easy styrene diffusion, efficient debromination, selection of aromatic compounds, and decomposition of styrene and BTE compounds [35,70]. After the reaction and decomposition of UPR into styrene and BTE compounds, a short fibre mixed with the catalyst remained in the last stage as a solid residue without any degeneration because of its higher melting temperature [11].

3.4. Kinetic analysis

The activation energy (Ea) values of WTB catalytic pyrolysis at specific conversion (y) were computed using the slope of model-free KAS, FWO, and Friedman plots, as shown in Fig. 7. The calculations revealed that ZSM-5/WTB sample had Ea of 126 kJ/mol (KAS), 160 kJ/mol (FWO), and 171 kJ/mol (Friedman) vs 102 kJ/mol (KAS), 132 kJ/mol (FWO), and 99 kJ/mol (Friedman) in case of Y-type/WTB sample. The Ea values in different conversion zones for both samples are displayed in Fig. 8. The relationship showed that the values obtained from model-free KAS, FWO, and Friedman methods appear to have a nearly comparable trend in all conversion regions with a little alteration between models due to natural working mechanism and assumptions of each model. Also, Friedman technique showed a little different trend due to its highly sensitive noise data, hence affecting the computed Ea

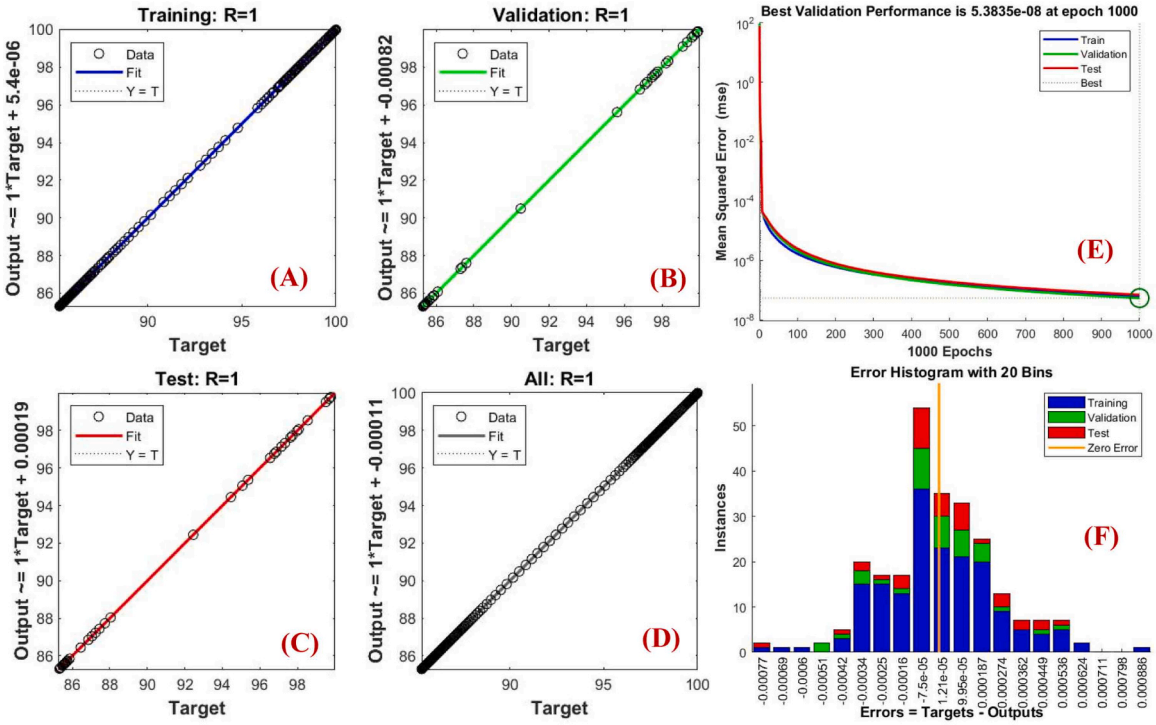

Fig. 10. The ANN predicted diagrams of ZSM-5/WTB pyrolysis at 10 °C/min.

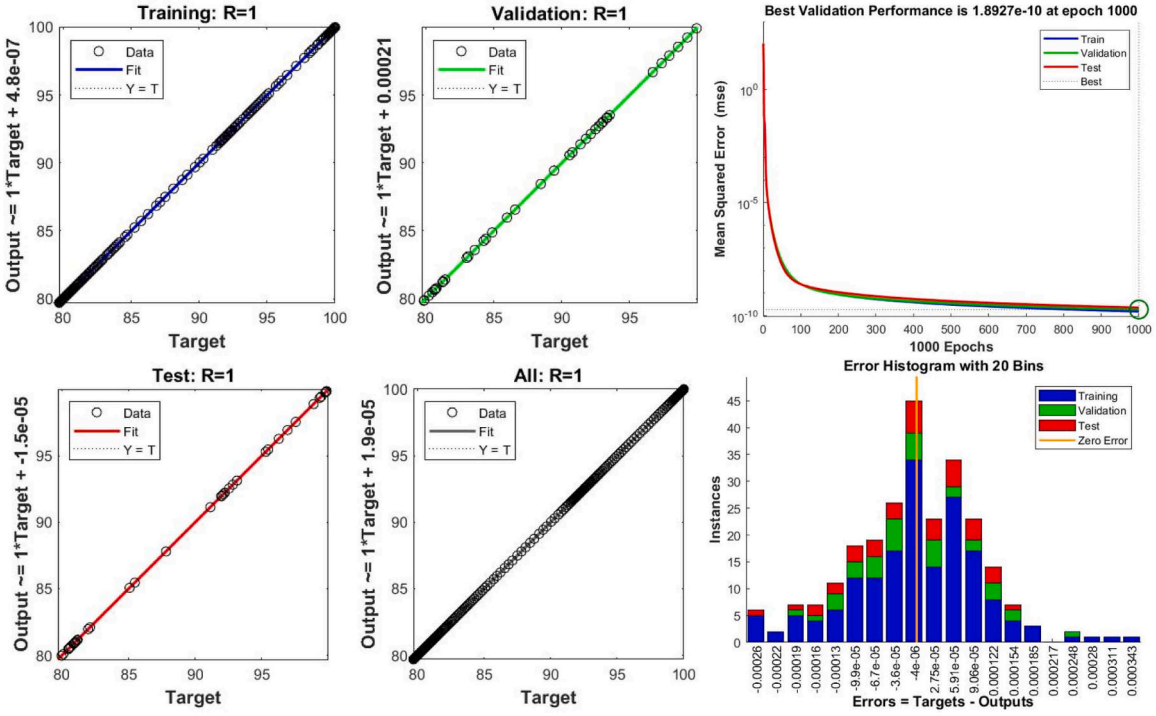

Fig. 11. The ANN predicted diagrams of Y-type/WTB pyrolysis at 10 °C/min.

values [44]. All these computed Ea values and their R^2 (correlation coefficient) value are presented in Table 4. As shown, R^2 average values were above 0.91 (in case of FWO), what proves its usefulness for evaluation of TGA experimental results. Also, it was noticed that lower Ea values were found at the beginning of conversion process (y = 0.1) due to the conversion process started using pyrolysis. Usually, it starts with moisture evaporation and breakdown of compounds with small molecular weight, thus needing lower energy, while in case of reaction progressing, the required Ea increases because several sub-components are involved in the reaction what makes the reaction more complex and in need of more energy to break complex compounds and decompose them in a single-step reaction [29]. Also, some big variation in R^2 values was observed at the lower conversion rates due to fact that several reactions take a place in parallel and intermediate products [30],

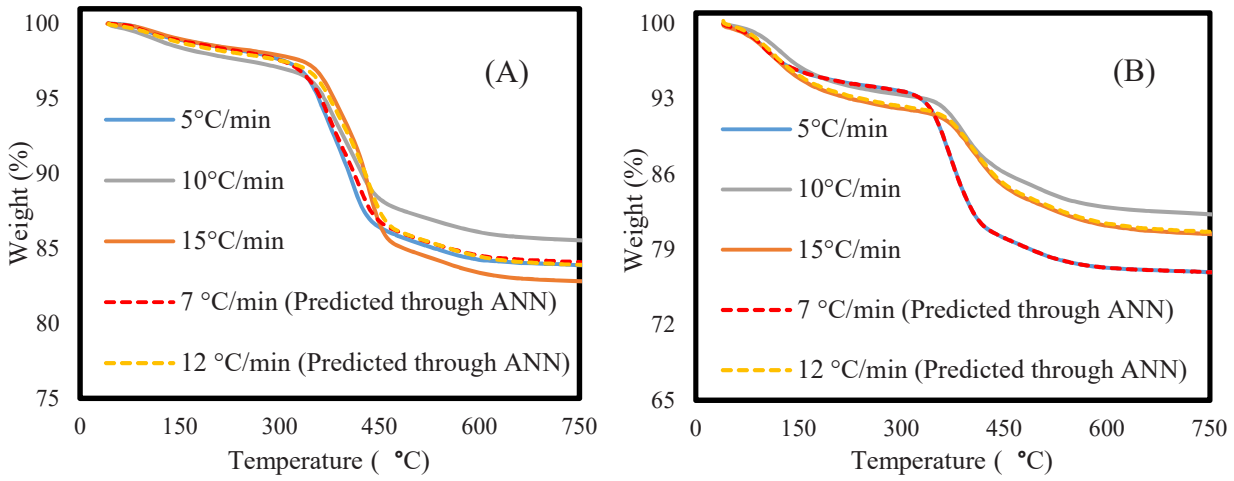

Fig. 12. The experimental TGA and ANN-predicted TGA curve for A) ZSM-5/WTB and B) Y-type/WTB samples at various heating rates.

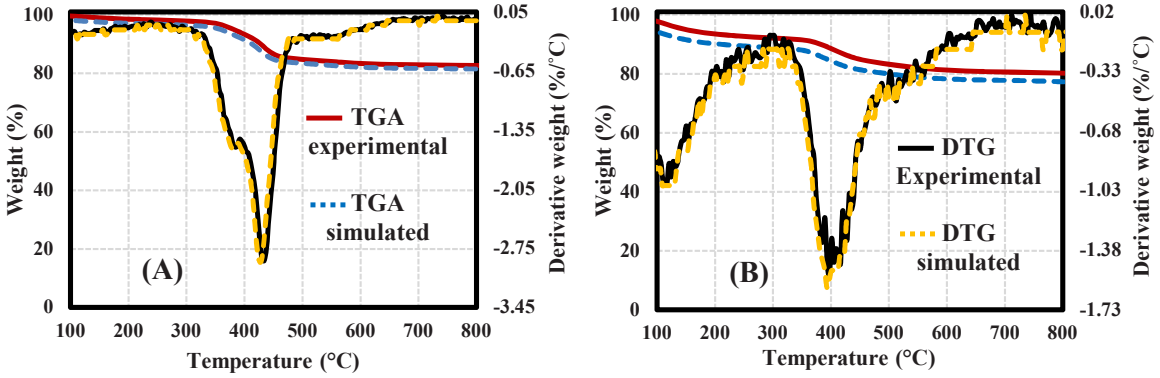

Fig. 13. Fitting of TGA and DTG curves of WTB pyrolysis over (A) ZSM-5 and (B) Y-type catalyst at 15 °C/min.

Table 6
DAEM and IPR optimum parameters of WTB catalytic pyrolysis samples.

Parameter	ZSM-5		Y-type	
	DAEM	IPR	DAEM	IPR
E1	209.995	136.576	131.356	85.431
A1	8.13E + 13	1.35E + 09	6.51E + 17	1.087E + 13
E2	150.394	142.03	94.0746	88.848
A2	8.14E + 26	3.11E + 23	6.51E + 30	2.49E + 27

what makes the mechanism of reaction is more complex and hard to capture all of them accurately using such these types of kinetic models that mostly used to simulate the main conversion region (0.4–0.8%) [11, 30], what lead to poor fit to the experimental data and R^2 as well. Since both of catalysts have a different structure and composition that can effect on the mechanism of reaction, the lower value shifted a little till 0.4. Also, noisily data and uncertainties in experimental data can be another reason [41,42]. Also, the simplifying assumptions of these models can effect on equally of fitting [12]. Finally and compared to average Ea of WTB pyrolysis (182–228 kJ/mol) [30], the catalytic pyrolysis of WTB has a very low Ea, which means that the reaction's complexity is significantly reduced.

Vyazovkin and Cai models do not need any mathematical assumptions and Ea values can be computed by optimising the process (numerical integration algorithms) by minimising the object function. The algorithms were built using Matlab software with Ea = 200 kJ/mol as initial boundaries. The code was run for several times until the Ea values became constant, thus referring to optimal values and all iterations are shown in the supplementary materials section, Table S1. As shown, the optimal values of average Ea were estimated at 126 kJ/mol with R^2 above 0.90 (ZSM-5) and 100–104 kJ/mol with $R^2 = 0.90$ (Y-type). Based on the parameters obtained from the optimal conditions for each sample, Vyazovkin and Cai plots were constructed, and the plots are shown in Fig. 9, while their Y-axes were defined using Equation (1S and 2S) in the supplementary materials. Also, the thermodynamic parameters of ZSM-5/WTB (at 10 °C/min) and Y-type/WTB samples (at 15 °C/min) were calculated based on Eqs. (9)–(12) and the results are shown in Table 5.

3.5. ANN-based prediction of pyrolytic behaviour

The main goal of using ANN model in the present research to predict the weight loss curve of unknown samples, that why we selected two heating rates did not measured. The build ANN model was applied to predict TGA experimental data of WTB samples at unknown heating rates with different zeolite catalysts. The results showed that two hidden layers in a 3 × 5 × 1 pattern were the best conditions and the performance and features of the developed ANN model for both samples are shown in Figs. 10 and 11. Based on these conditions, the training part of ANN model was successful in prediction of thermal behaviour of WTB samples over zeolite catalysts with $R^2 = 1$, as shown in Figs. 10A and 11A. The training results of each WTB sample were validated by comparing them with the experimental thermogravimetric data

received at the reported heating rates, which showed a complete match (Figs. 10B, 11B). Also, during the optimisation process, the network accuracy error distribution was observed at each step and regressions showed a high level of accuracy, as displayed in Fig. 10C and D) and Fig. 11C and D). Meanwhile, the minimum square error obtained was 5.383 E-08 in case of ZSM-5 (Fig. 10E) and 1.8927 E-10 in case of Y-type (Fig. 11E) after 1000 iterations. The histogram error distribution diagram (Figs. 10F and 11F) showed a wide range of datasets following normal distribution approach around zero and located in the ranges of $-0.00077 + 0.000886$ (ZSM-5) and $-0.00026 + 0.000343$ (Y-type). The built ANN model and the weight loss (%) curve for both WTB samples at 7 and 12 °C/min rate were predicted and all experimental TGA and ANN-predicted TGA curves are shown in Fig. 12. As shown, the ANN model was used effectively for learning and prediction of the weight loss behaviour of WTB samples at unknown heating conditions. These results indicating a well-trained network can be used to predict more data.

Finally, the thermal degradation regions of TGA and DTG experimental curves of zeolite catalysts/WTB samples were fitted mathematically using DAEM and IPR, respectively. Fig. 13 shows the fitted curves at some heating rate (15 °C/min) which were validated by comparing them with experimental TGA-DTG data to investigate the model's accuracy. The solid red and blue dashed lines in the figure are experimental and simulated TGA data respectively, while the straight black line and yellow dashed lines are both experimental and simulated DTG data respectively. The optimum conditions used in the fitting process (activation energies and pre-exponential) are described in Table 6. The results showed a strong agreement between the fitting data and the actual thermal behaviour of zeolite catalysts/WTB samples during catalytic pyrolysis process with deviation close to 0.

4. Conclusions

In the present work, the catalytic pyrolysis behaviour of WTB (fibreglass/unsaturated polyester resin) over ZSM-5 and Y-type zeolite catalysts and their volatile products were studied and characterised. The kinetic characteristics and thermodynamic behaviour of the catalytic process were also studied. Besides, thermal degradation curves were fitted mathematically and an artificial neural network (ANN) model was built to predict degeneration zones at unknown heating rates. The TGA and GC/MS results showed that the resin fraction of WTB decomposed completely into value-added aroma chemicals mainly consisting of benzene, toluene, and ethylbenzene (BTE) with abundance of 64% at 15 °C/min (Y-type) and 36.31% at 10°C/min (ZSM-5). Meanwhile, the kinetic results showed that the catalytic process can contribute significantly to reduction of the reaction complexity with estimated average activation energies in the ranges of 126–171 kJ/mol (ZSM-5) and 99–132 kJ/mol (Y-type). The developed ANN model showed a distinguished performance in prediction of thermal decomposition of WBT at unknown heating conditions with $R^2 = 1$. Therefore, it can be said that catalytic pyrolysis and ANN have high potential in cracking styrene (the main compound of polyester resins) into BTE compounds and predicting their thermal behaviour. Finally, the developed ANN model can be used to simulate and predict the complex pyrolysis process of WTB and pyrolysis of different zones with unknown heating rates without the need to perform further heating rate TG measurements, saving time and cost.

CRediT authorship contribution statement

Justas Eimontas: Conceptualization, Data curation, Formal analysis, Methodology. **Samy Yousef:** Conceptualization, Data curation, Formal analysis, Funding acquisition, Investigation, Methodology, Project administration, Resources, Software, Supervision, Validation, Visualization, Writing – original draft, Writing – review & editing. **Mohammed Ali Abdelnaby:** Conceptualization, Data curation, Formal analysis, Methodology, Software, Validation, Writing – original draft. **Nerijus Striūgas:** Conceptualization, Data curation, Formal analysis, Funding acquisition.

Declaration of Competing Interest

The authors declare that they have no known competing financial interests or personal relationships that could have appeared to influence the work reported in this paper.

Data availability

The data that has been used is confidential.

Acknowledgement

This project has received funding from the Research Council of Lithuania (LMTLT), agreement No. S-MIP-23–118.

Appendix A. Supporting information

Supplementary data associated with this article can be found in the online version at doi:10.1016/j.jaap.2023.106330.

References

[1] P. Majewski, N. Florin, J. Jit, R.A. Stewart, End-of-life policy considerations for wind turbine blades, Renew. Sustain. Energy Rev. (2022), https://doi.org/10.1016/j.rser.2022.112538.
[2] J. Beauson, A. Laurent, D.P. Rudolph, J. Pagh Jensen, The complex end-of-life of wind turbine blades: a review of the european context, Renew. Sustain. Energy Rev. (2022), https://doi.org/10.1016/j.rser.2021.111847.
[3] B. Diez-Cañamero, J.M.F. Mendoza, Circular economy performance and carbon footprint of wind turbine blade waste management alternatives, Waste Manag. (2023), https://doi.org/10.1016/j.wasman.2023.03.041.
[4] K.W. Lund, M.L. Nielsen, E.S. Madsen, Sustainability assessment of new technologies using multi criteria decision making: a framework and application in sectioning end-of-life wind turbine blades, Renew. Sustain. Energy Rev. (2023), https://doi.org/10.1016/j.rser.2023.113542.
[5] N. Cong, Y. Song, M. Zhang, W. Wu, Life cycle assessment of carbon reduction potential of EoL wind turbine blades disposal scenarios in China, Environ. Impact Assess. Rev. (2023), https://doi.org/10.1016/j.eiar.2023.107072.
[6] P. Liu, F. Meng, C.Y. Barlow, Wind turbine blade end-of-life options: an economic comparison, Resour. Conserv. Recycl. (2022), https://doi.org/10.1016/j.resconrec.2022.106202.
[7] J. Eimontas, N. Striūgas, M. Praspaliauskas, M.A. Abdelnaby, Pyrolysis kinetic behaviour of glass fibre-reinforced epoxy resin composites using linear and nonlinear isoconversional methods, Polymers (2021), https://doi.org/10.3390/polym13101543.
[8] J. Eimontas, N. Striūgas, S.P. Subadra, M.A. Abdelnaby, Thermal degradation and pyrolysis kinetic behaviour of glass fibre-reinforced thermoplastic resin by TG-FTIR, Py-GC/MS, linear and nonlinear isoconversional models, J. Mater. Res. Technol. (2021), https://doi.org/10.1016/j.jmrt.2021.11.011.
[9] S. Yousef, J. Eimontas, N. Striūgas, M.A. Abdelnaby, Influence of carbon black filler on pyrolysis kinetic behaviour and TG-FTIR-GC–MS analysis of glass fibre reinforced polymer composites, Energy (2021), https://doi.org/10.1016/j.energy.2021.121167.
[10] N. Striūgas, J. Eimontas, M.A. Abdelnaby, Thermal decomposition of CNTs and graphene-reinforced glass fibers/epoxy and their kinetics, Biomass Convers. Biorefinery (2022), https://doi.org/10.1007/s13399-022-02341-3.
[11] I. Kiminaitė, J. Eimontas, N. Striūgas, M.A. Abdelnaby, Catalytic pyrolysis kinetic behaviour of glass fibre-reinforced epoxy resin composites over ZSM-5 zeolite catalyst, Fuel (2022), https://doi.org/10.1016/j.fuel.2022.123235.
[12] S. Yousef, I. Kiminaitė, J. Eimontas, N. Striūgas, M.A. Abdelnaby, Recovery of phenol and acetic acid from glass fibre reinforced thermoplastic resin using catalytic pyrolysis process on ZSM-5 zeolite catalyst and its kinetic behaviour, Thermochim. Acta (2022), https://doi.org/10.1016/j.tca.2022.179293.
[13] M. Praspaliauskas, J. Eimontas, N. Striūgas, M.A. Abdelnaby, Catalytic pyrolysis and kinetic study of glass fibre-reinforced epoxy resin over CNTs, graphene and carbon black particles/ZSM-5 zeolite hybrid catalysts, J. Therm. Anal. Calorim. (2023), https://doi.org/10.1007/s10973-022-11776-9.
[14] Y. Ren, L. Xu, X. Shang, Z. Shen, R. Fu, W. Li, L. Guo, Evaluation of mechanical properties and pyrolysis products of carbon fibers recycled by microwave pyrolysis, ACS Omega (2022), https://doi.org/10.1021/acsomega.1c06652.
[15] L. Ge, X. Li, H. Feng, Xu, Chunyao, Y. Lu, B. Chen, D. Li, Xu, Chang, Analysis of the pyrolysis process, kinetics and products of the base components of waste wind turbine blades (epoxy resin and carbon fiber, J. Anal. Appl. Pyrolysis (2023), https://doi.org/10.1016/j.jaap.2023.105919.

[16] L. Ge, Chunyao Xu, H. Feng, H. Jiang, X. Li, Y. Lu, Z. Sun, Y. Wang, Xu, Chang, Study on isothermal pyrolysis and product characteristics of basic components of waste wind turbine blades, J. Anal. Appl. Pyrolysis (2023), https://doi.org/10.1016/j.jaap.2023.105964.

[17] W. Chen, M. Ye, M. Li, B. Xi, J. Hou, X. Qi, J. Zhang, Y. Wei, F. Meng, Characteristics, kinetics and product distribution on pyrolysis process for waste wind turbine blades, J. Anal. Appl. Pyrolysis (2023), https://doi.org/10.1016/j.jaap.2023.105859.

[18] I.B.C.M. Rocha, S. Raijmaekers, R.P.L. Nijssen, F.P. van der Meer, L.J. Sluys, Hygrothermal ageing behaviour of a glass/epoxy composite used in wind turbine blades, Compos. Struct. (2017), https://doi.org/10.1016/j.compstruct.2017.04.028.

[19] M. xin Xu, H. wen Ji, Y. chang Wu, J. yi Di, X. xi Meng, H. Jiang, Q. Lu, The pyrolysis of end-of-life wind turbine blades under different atmospheres and their effects on the recovered glass fibers, Compos. Part B Eng. (2023), https://doi.org/10.1016/j.compositesb.2022.110493.

[20] Y. Wu, Z. Ge, C. Huang, Z. Zha, M. Zeng, Y. Ma, L. Sun, Z. Hou, S. Chu, H. Zhang, In-situ pyrolysis kinetic analysis and fixed-bed pyrolysis behavior of ex-service wind turbine blades, Waste Manag. (2023), https://doi.org/10.1016/j.wasman.2023.05.049.

[21] L. Mishnaevsky, K. Branner, H.N. Petersen, J. Beauson, M. McGugan, B.F. Sørensen, Materials for wind turbine blades: an overview, Materials 10 (2017) 1285, https://doi.org/10.3390/ma10111285.

[22] Y. Wu, Z. Ge, C. Huang, Z. Zha, Z. Hou, S. Chu, Y. Ma, H. Zhang, L. Sun, M. Zeng, In-situ pyrolysis kinetic analysis and fixed-bed pyrolysis behavior of ex-service wind turbine blades, Waste Manag. (2023), https://doi.org/10.1016/j.wasman.2023.05.049.

[23] H.W. Ji, J. Yang, J.Y. Di, Q. Lu, M.X. Xu, X.X. Meng, Y.C. Wu, H. Jiang, Effects of core materials on the evolution of products during the pyrolysis of end-of-life wind turbine blades, J. Anal. Appl. Pyrolysis (2023), https://doi.org/10.1016/j.jaap.2023.106222.

[24] M.X. Xu, J.Y. Di, X.X. Meng, H. Jiang, Q. Lu, J.H. Li, Y.C. Wu, H. Ji, Insights into the pyrolysis mechanisms of epoxy resin polymers based on the combination of experiments and ReaxFF-MD simulation, Chem. Eng. J. (2023), https://doi.org/10.1016/j.cej.2023.145404.

[25] B. Wang, X. Wang, Y. Shen, Y. Liu, Z. Hu, N. Xu, F. Lu, Y. Huang, Recycling of carbon fibers from unsaturated polyester composites via a hydrolysis oxidation synergistic catalytic strategy, Compos. Sci. Technol. (2021), https://doi.org/10.1016/j.compscitech.2020.108589.

[26] M.A.M. Khorasani, S. Sahebian, A. Zabett, Effects of toughened polyester on fatigue behavior of glass fiber reinforced polyester composite for wind turbine blade, Polym. Compos. (2020), https://doi.org/10.1002/pc.25808.

[27] K. Aalto-Korte, K. Suuronen, Occupational contact allergy to components of polyester resin systems, Contact Dermat. 75 (2016) 14–19.

[28] C. Higgins, J. Cahill, R. Jolanki, R. Nixon, Polyester resins, in: S. John, J. Johansen, T. Rustemeyer, P. Elsner, H. Maibach (Eds.), Kanerva's Occupational Dermatology, Springer, Cham, 2020, https://doi.org/10.1007/978-3-319-68617-2_54.

[29] S. Yousef, J. Eimontas, N. Striūgas, M.A. Abdelnaby, Pyrolysis kinetic behaviour and thermodynamic analysis of waste wind turbine blades (carbon fibres/unsaturated polyester resin, Energy Sources Part A Recovery Util. Environ. Eff. (2023), https://doi.org/10.1080/15567036.2023.2246422.

[30] S. Yousef, J. Eimontas, N. Striūgas, M.A. Abdelnaby, Recovery of styrene from waste wind turbine blades (fiberglass/polyester resin composites) using pyrolysis treatment and its kinetic behavior, J. Therm. Anal. Calorim. (2023), https://doi.org/10.1007/s10973-023-12714-z.

[31] K. Zakarauskas, J. Eimontas, N. Striūgas, Recovery of styrene-rich oil and glass fibres from fibres-reinforced unsaturated polyester resin end-of-life wind turbine blades using pyrolysis technology, J. Anal. Appl. Pyrolysis (2023), https://doi.org/10.1016/j.jaap.2023.106100.

[32] European Chemicals Agency: Styrene Infocard. https://www.echa.europa.eu/substance-information/-/substanceinfo/100.002.592.

[33] J. Huff, P.F. Infante, Styrene exposure and risk of cancer, Mutagenesis 26 (5) (2011) 583–584.

[34] A. Verma, S. Sharma, H. Pramanik, Pyrolysis of waste expanded polystyrene and reduction of styrene via in-situ multiphase pyrolysis of product oil for the production of fuel range hydrocarbons, Waste Manag. (2021), https://doi.org/10.1016/j.wasman.2020.11.035.

[35] A.C. Dyer, M.A. Nahil, P.T. Williams, Biomass: polystyrene co-pyrolysis coupled with metal-modified zeolite catalysis for liquid fuel and chemical production, J. Mater. Cycles Waste Manag. 24 (2022) 477–490, https://doi.org/10.1007/s10163-021-01334-0.

[36] Y.M. Kim, T.U. Han, S. Kim, J. Jae, J.K. Jeon, S.C. Jung, Y.K. Park, Catalytic co-pyrolysis of epoxy-printed circuit board and plastics over HZSM-5 and HY, J. Clean. Prod. (2017), https://doi.org/10.1016/j.jclepro.2017.08.224.

[37] A.M. Gonzalez-Aguilar, V. Pérez-García, J.M. Riesco-Ávila, A thermo-catalytic pyrolysis of polystyrene waste review: a systematic, statistical, and bibliometric approach, Polymers (2023), https://doi.org/10.3390/polym15061582.

[38] R. Mishra, A. Kumar, E. Singh, S. Kumar, Recent research advancements in catalytic pyrolysis of plastic waste, ACS Sustain. Chem. Eng. (2023), https://doi.org/10.1021/acssuschemeng.2c05759.

[39] B. Gajera, U. Tyagi, A.K. Sarma, et al., Pyrolysis of cattle manure: kinetics and thermodynamic analysis using TGA and artificial neural network, Biomass Convers. Biorefinery (2023), https://doi.org/10.1007/s13399-023-04476-3.

[40] J. Eimontas, N. Striugas, M.A. Abdelnaby, Modeling of metalized food packaging plastics pyrolysis kinetics using an independent parallel reactions kinetic model, Polymers (2020), https://doi.org/10.3390/polym12081763.

[41] K. Zakarauskas, J. Eimontas, N. Striūgas, A new sustainable strategy for oil, CH4 and aluminum recovery from metallised food packaging plastics waste using catalytic pyrolysis over ZSM-5 zeolite catalyst, Thermochim. Acta (2022), https://doi.org/10.1016/j.tca.2022.179223.

[42] J. Eimontas, A. Jančauskas, K. Zakarauskas, N. Striūgas, L. Vorotinskienė, Investigation of optimal temperature for thermal catalytic conversion of marine biomass for recovery of higher-added-value energy products, Energies (2023), https://doi.org/10.3390/en16083457.

[43] M. Abdelnaby, J. Eimontas, N. Striūgas, K. Zakarauskas, M.A. Praspaliauskas, Pyrolysis kinetic behavior and TG-FTIR-GC–MS analysis of metallised food packaging plastics, Fuel (2020), https://doi.org/10.1016/j.fuel.2020.118737.

[44] A. Mohamed, J. Eimontas, N. Striūgas, M. Ali Abdelnaby, Pyrolysis kinetic behavior and TG-FTIR-GC–MS analysis of end-life ultrafiltration polymer nanocomposite membranes, Chem. Eng. J. (2022), https://doi.org/10.1016/j.cej.2021.131181.

[45] K. Açıkalın, Determination of kinetic triplet, thermal degradation behaviour and thermodynamic properties for pyrolysis of a lignocellulosic biomass, Bioresour. Technol. (2021), https://doi.org/10.1016/j.biortech.2021.125438.

[46] J. Eimontas, S. Yousef, N. Striūgas, M.A. Abdelnaby, Catalytic pyrolysis kinetic behaviour and TG-FTIR-GC–MS analysis of waste fishing nets over ZSM-5 zeolite catalyst for caprolactam recovery, Renew. Energy (2021), https://doi.org/10.1016/j.renene.2021.07.143.

[47] M.A. Abdelnaby, J. Eimontas, N. Striūgas, Pyrolysis and gasification kinetic behavior of mango seed shells using TG-FTIR-GC–MS system under N2 and CO_2 atmospheres, Renew. Energy (2021), https://doi.org/10.1016/j.renene.2021.04.034.

[48] S. Yousef, J. Eimontas, N. Striūgas, M. Praspaliauskas, M.A. Abdelnaby, Pyrolysis kinetic behaviour, TG-FTIR, and GC/MS analysis of cigarette butts and their components, Biomass Convers. Biorefinery (2022), https://doi.org/10.1007/s13399-022-02698-5.

[49] N. Striūgas, J. Eimontas, M.A. Abdelnaby, Pyrolysis kinetic behaviour and TG-FTIR-GC–MS analysis of Coronavirus Face Masks, J. Anal. Appl. Pyrolysis (2021), https://doi.org/10.1016/j.jaap.2021.105118.

[50] A. Mohamed, J. Eimontas, N. Striūgas, M.A. Abdelnaby, Morphology, compositions, thermal behavior and kinetics of pyrolysis of lint-microfibers generated from clothes dryer, J. Anal. Appl. Pyrolysis (2021), https://doi.org/10.1016/j.jaap.2021.105037.

[51] J. Eimontas, N. Striūgas, M.A. Abdelnaby, S. Yousef, Catalytic pyrolysis kinetic behavior and TG-FTIR-GC–MS analysis of metallized food packaging plastics with different concentrations of ZSM-5 zeolite catalyst, Polymers (2021), https://doi.org/10.3390/polym13050702.

[52] M. Praspaliauskas, J. Eimontas, N. Striūgas, A. Mohamed, M.A. Abdelnaby, Phenol and benzoic acid recovery from end-of-life of polysulfone ultrafiltration membranes and its thermochemical kinetic behaviour, Energy Sources Part A Recovery Util. Environ. Eff. (2023), https://doi.org/10.1080/15567036.2023.2213669.

[53] M. Ali Abdelnaby, J. Eimontas, N. Striūgas, A. Mohamed, Pyrolysis kinetic behavior and thermodynamic analysis of pet nonwoven fabric, Materials (2023), https://doi.org/10.3390/ma16186079.

[54] A. Nawaz, P. Kumar, Thermal degradation of hazardous 3-layered COVID-19 face mask through pyrolysis: kinetic, thermodynamic, prediction modelling using ANN and volatile product characterization, J. Taiwan Inst. Chem. Eng. (2022), https://doi.org/10.1016/j.jtice.2022.104538.

[55] Sharath P. Subadra, Simona Tuckute, Ar.ūnas Baltušnikas, Stasė.-Irena Lukošiūtė, E. l Arafa, Alaa Mohamed, Finite element analysis of fibreglass and carbon fabrics reinforced polyethersulfone membranes, Mater. Today Commun. (2022), https://doi.org/10.1016/j.mtcomm.2022.103682.

[56] P. Yan, I.N. Azreena, H. Peng, H. Rabiee, M. Ahmed, Y. Weng, Z. Zhu, E. M. Kennedy, M. Stockenhuber, Catalytic hydropyrolysis of biomass using natural zeolite-based catalysts, Chem. Eng. J. (2023), https://doi.org/10.1016/j.cej.2023.146630.

[57] M. Li, Y.S. Zhang, S. Cheng, B. Qu, A. Li, F. Meng, G. Ji, The impact of heating rate on the decomposition kinetics and product distribution of algal waste pyrolysis with in-situ weight measurement, Chem. Eng. J. (2023), https://doi.org/10.1016/j.cej.2023.141368.

[58] T. Kassa Dada, A. Vuppaladadiyam, A. Xiaofei Duan, R. Kumar, E. Antunes, Probing the effect of Cu-SrO loading on catalyst supports (ZSM-5, Y-zeolite, activated carbon, Al2O3, and ZrO2) for aromatics production during catalytic co-pyrolysis of biomass and waste cooking oil, Bioresour. Technol. (2022), https://doi.org/10.1016/j.biortech.2022.127515.

[59] C.F. Bustillo-Lecompte, D. Kakar, M. Mehrvar, Photochemical treatment of benzene, toluene, ethylbenzene, and xylenes (BTEX) in aqueous solutions using advanced oxidation processes: towards a cleaner production in the petroleum refining and petrochemical industries, J. Clean. Prod. (2018), https://doi.org/10.1016/j.jclepro.2018.03.135.

[60] Bin Tian, Ying–yun Qiao, Yuan–yu Tian, Qing Liu, Investigation on the effect of particle size and heating rate on pyrolysis characteristics of a bituminous coal by TG–FTIR, J. Anal. Appl. Pyrolysis (2016), https://doi.org/10.1016/j.jaap.2016.08.020.

[61] F. xiang Xu, Xu. Zhang, Li. qun Jiang, H. bin Li, Z. li Zhao, F. Zhang, TG-FTIR for kinetic evaluation and evolved gas analysis of cellulose with different structures, Fuel (2020), https://doi.org/10.1016/j.fuel.2020.117365.

[62] J. Jiang, Z. Zhong, H. Xia, S. Pang, Mi. Li, R. Ruan, A.J. Ragauskas, J. Wang, Y. Sun, Xi. Wang, G. Liu, K. Wang, J. Xu, Recycling benzene and ethylbenzene from in-situ catalytic fast pyrolysis of plastic wastes, Energy Convers. Manag. (2019), https://doi.org/10.1016/j.enconman.2019.112088.

[63] A. López, I. de Marco, B.M. Caballero, M.F. Laresgoiti, A. Adrados, A. Aranzabal, Catalytic pyrolysis of plastic wastes with two different types of catalysts: ZSM-5 zeolite and Red Mud, Appl. Catal. B Environ. (2011), https://doi.org/10.1016/j.apcatb.2011.03.030.
[64] H. Peng, P. Li, Q. Yang, Pyrolysis of polyester and viscose fiber over ZSM-5: synergistic effect and distribution of products, J. Therm. Anal. Calorim. 147 (2022) 12535–12545, https://doi.org/10.1007/s10973-022-11521-2.
[65] P.G. Junqueira, I.N. Caxiano, P.V. Mangili, D.M. Prata, Environ-economic analysis of conceptual intensification alternatives applied to the ethylbenzene production, Comput. Chem. Eng. (2020), https://doi.org/10.1016/j.compchemeng.2020.106783.
[66] L. Mishnaevsky, K. Branner, H.N. Petersen, J. Beauson, M. McGugan, B.F. Sørensen, Materials for wind turbine blades: an overview, Materials 10 (11) (2017) 1285, https://doi.org/10.3390/ma10111285.
[67] K. Laoubi, Z. Hamadi, A. Ahmed Benyahia, A. Serier, Z. Azari, Thermal behavior of E-glass fiber-reinforced unsaturated polyester composites, Compos. Part B Eng. (2014), https://doi.org/10.1016/j.compositesb.2013.08.085.
[68] P. Yan, H. Wang, Y. Liao, C. Wang, Zeolite catalysts for the valorization of biomass into platform compounds and biochemicals/biofuels: a review, Renew. Sustain. Energy Rev. (2023), https://doi.org/10.1016/j.rser.2023.113219.
[69] N. Miskolczi, T. Juzsakova, J. Sója, Preparation and application of metal loaded ZSM-5 and y-zeolite catalysts for thermo-catalytic pyrolysis of real end of life vehicle plastics waste, J. Energy Inst. (2019), https://doi.org/10.1016/j.joei.2017.10.017.
[70] O.D. Mante, F.A. Agblevor, S.T. Oyama, R. McClung, Catalytic pyrolysis with ZSM-5 based additive as co-catalyst to Y-zeolite in two reactor configurations, Fuel (2014), https://doi.org/10.1016/j.fuel.2013.09.034.